The Mechanism of Na^+/K^+ Selectivity in Mammalian Voltage-Gated Sodium Channels Based on Molecular Dynamics Simulation

Mengdie Xia,[†△] Huihui Liu,[†△] Yang Li,[†△] Nieng Yan,[‡] and Haipeng Gong[†]*

[†]MOE Key Laboratory of Bioinformatics, School of Life Sciences and [‡]State Key Laboratory of Biomembrane and Membrane Biotechnology, School of Medicine, Tsinghua University, Beijing, China

Submitted February 18, 2013, and accepted for publication April 19, 2013.

[△]Mengdie Xia, Huihui Liu, and Yang Li contributed equally to this work.

*Correspondence: hgong@tsinghua.edu.cn

Detailed information for simulation methods

Model definition and basic simulation parameters

The protein structure was processed in a similar way to our previous work (1). Atomic coordinates of Na_vRh channel were taken from the Protein Data Bank (PDB code: 4DXW). After removal of the voltage-sensing domains, the pore domain (residue 118-228 in all chains) was inserted into POPC bilayer (about 187 molecules) for simulation. Finally, the system was immersed in TIP3P explicit water (about 16000 water molecules) and electrostatically neutralized by 70 mM XCl, where X corresponds to Na^+, K^+, or their combination. Mutation on the protein structure was accomplished by the "Mutator" plugin of VMD 1.9.1 (2). To avoid the negative influence generated by the removal of the voltage-sensing domains from the protein, the N-terminal S4-5 helices (residue 118-123) were positionally restrained by 5 kcal/mol/$Å^2$ in all systems. All simulations were performed by NAMD 2.8 (3) in an NPT ensemble using the CHARMM27 force field with CMAP correction (4) and NBFIX (5). The pressure and temperature were held at 1 atm and 310 K by the Nose-Hoover Langevin piston (6,7) and the Langevin thermostat (7) respectively. The van der Waals interaction was smoothly switched to zero from 10 to 12 Å, and all interations beyond 12 Å were ignored from energy calculation. Periodic boundary conditions (PBC) was applied to avoid the edge effect and the electrostatic potential was solved using the Particle Mesh Ewald (PME) (8).

The equilibrium simulation

The WT-Na_vRh system was pre-equilibrated in the same three-stage protocol as our previous research (1). When simulating the mutant Na_vRh, the protocol was adapted to four stages to guarantee the stability of the system after mutation. In the first stage, all atoms except those belonging to the lipid tails were fixed and the system was minimized by 2000 steps and then equilibrated for 0.5 ns to relax the lipid-protein interaction. In the second stage, protein atom and ions were harmonically restrained with a force constant of 5 kcal/mol/$Å^2$, and the sytem was minimized by 2000 steps and then equilibrated for 2 ns to relax the protein-water interaction. In the

third stage, the constraints on protein and ions were reduced to 1 kcal/mol/Å^2, and the system was further relaxed for 2 ns. In the final stage, the system was equilibrated for 5 ns with all constraints released. After the pre-equlibration, 50 ns or 30 ns productive simulations were conducted for each system (Table S1), using an integration time of 2 fs, where the hydrogen atoms were restrained by the SETTLE algorithm (9) and the area of membrane was held constant. In total, 13 equilibrium simulations were conducted and their details were shown in Table S1. According to the root-mean-square-distance (RMSD) analysis (Fig. S19), all systems are stable during the simulation, with RMSD < 2.5 Å.

In the simulation of the DEKA mutant, the status of Lys180 side-chain was affected by random factors. As described in the Results, Lys180 was at the "off-state" to prohibit ion permeation in simulation 6 and 8 (in Table S1). In other simulations not listed in Table S1, the Lys180 was at the "on-state", which allowed the ion passage. Therefore, the Lys180 side-chain was forced to the "on-state" in the later simulation (simulation 5, 7, 9, 10, and 13 in Table S1). More specifically, a force constant of 100 kcal/mol/Å^2 was applied to constrain the distance between the side-chain nitrogen of Lys180 (chain C) and the center of carboxylate oxygens of Glu183 (chain D) to be less than 3.5 Å.

The adaptive biasing force (ABF) simulation

The potential of mean force (PMF) was calculated by the ABF method (10-13). In all ABF simulations, the time step was chosen as 1fs. All other parameters were identical to the equilibrium simulations.

In the one-dimensional ABF calculation (Fig. S8 and Fig. S11), the distance between the sampling ion and the center of all α-carbons in the SF (residue 178-183) projected on z-axis (the axis perpendicular to the membrane plane) was chosen as the reaction coordinate, which was further divided into 2 to 5 windows, each spanning 1 to 5 Å. The initial structure in each window was taken from the equilibrium simulation in NaCl (simulation 5 in Table S1), in which the first Na^+ permeating across the SF and the successive one were chosen as the sampling ions for the

single-ion PMF curve (Fig. S8) and the PMF curve with the inner site pre-occupied (Fig. S11) respectively. To derive the according PMF curves for K^+, the sampling Na^+ was mutated to K^+. The systems were then minimized by 1000 steps and equilibrated for at least 1 ns. A force constant of 100 kcal/mol/Å^2 was applied to restrain the ion in each window, and the PMF was calculated in each window with a stepsize of 0.05 Å. In each step, 10000 samples were collected to roughly estimate the biasing force and the PMF curve was then updated every 2 or 4 ns. The calculation was conducted until convergence, when two successively updated PMF curves differed by less than 0.5 kcal/mol and the amount of sampling within each window differed by less than 5 fold. The latter criterion guarantees nearly uniform sampling along the reaction coordinate. Finally, the curves from all windows were spliced to generate the overall PMF curve. Totally 307 ns simulations were taken to generate the six one-dimensional PMF curves (Fig. S8 and Fig. S11). During the ABF simulation, only the sampling ion and the ion pre-positioned at the inner site were allowed to stay inside the SF, while all other cations were restricted more than 13 Å away from the extracellular SF entrance, which was defined by the geometric center of the backbone carbonyl carbons of Ser181. Furthermore, a force constant of 100 kcal/mol/Å^2 was applied to constrain the distance between the side-chain nitrogen of Lys180 (chain C) and the center of carboxylate oxygens of Glu183 (chain D) below 3.5 Å and above 4 Å respectively to maintain the on and off states of Lys180 side-chain.

In the two-dimensional ABF calculation (Fig. 3), the ion was forced to sample in the plane of the constriction site (as shown in Fig. S13C) perpendicular to the z-axis. Two orthogonal vectors within this plane were finally chosen as the reaction coordinates (as shown in Fig. 3A and Fig. 3B). The initial structures were taken from the equilibrium simulations of the DEKA mutant and the DEAA mutant in NaCl (simulation 5 and 11 in Table S1) respectively. In order to speed up calculation, only the SF region (residue 178 to 183) and the sampling Na^+ were preserved for later simulation. The SF structures were blocked at both N- and C-termini by acetyl and N-methyl-amide respectively and were immersed in a water box of 55 × 55 × 55 Å^3. Later, the negatively charged systems were electrostatically neutralized by explicit

Na^+ ions, which were restrained 13 Å away from the geometric center of the backbone carbonyl carbons of Ser181. A strong positional restraint (10 kcal/mol/Å^2) was applied on all α-carbons of the SF to maintain the backbone conformation. The Lys180 side-chain was constrained to the "on-state", as described above. In the system to estimate the K^+ free-energy map, all Na^+ ions were mutated to K^+. Before ABF simulations, all systems were minimized by 1000 steps and equilibrated for 4 ns. The sampling plane was then divided into at least four overlapping windows to enhance simulation efficiency. A force constant of 1000 kcal/mol/Å^2 was applied to restrain the ion in each window, and the PMF was calculated in each window with a binsize of 0.05 × 0.05 Å^2. In each bin, 10000 samples were collected to roughly estimate the biasing force and the PMF profile was then updated every 4 ns. The calculation was conducted until convergence, when two successively updated PMF maps differed by less than 0.2 kcal/mol. Finally, the PMF maps in all windows were merged to generate the overall 2-dimensional PMF profile. Totally 744 ns simulations were required to generate the four two-dimensional PMF profiles (Fig. 3C).

The free energy perturbation (FEP) simulation

In order to compare the binding affinities of Na^+ and K^+ at a site, the relative binding affinity $\Delta\Delta G(Na^+ \rightarrow K^+)$ was estimated by the free energy perturbation (FEP) (14,15) method. The time step in the FEP simulation was set to 1fs and the N-terminal S4-5 helices (residue 118-123) were positionally restrained by 1 kcal/mol/Å^2. All other parameters were identical to the equilibrium simulation. In all FEP calculations, the soft core potential (16) was adopted to attenuate the "end-point catastrophes" and intra-molecular interactions were decoupled from the FEP calculations. During the $Na^+ \rightarrow K^+$ mutation, a strong harmonic constraint (100 kcal/mol/Å^2) was applied to maintain the complete positional overlap of the vanishing Na^+ and appearing K^+. However, both ions are allowed to move freely within the allowed sampling space described specifically in each type of calculation in the following context. Similar to our previous research (1), the reaction coordinate was sufficiently stratified into numerous small windows (as demonstrated in Table S7), and the FEP simulations

were conducted in both the forward and the backward directions. The result was believed as convergent only when the probability distribution of energy changes in both directions, $P(\Delta E_{forward})$ and $P(-\Delta E_{backward})$, nearly completely overlapped in all windows. In this way, the overall free energy changes calculated from the forward and the backward processes never differed by more than 2.0 kcal/mol. Finally, by combining the forward and backward FEP simulations, Bennett acceptance ratio (BAR) estimator (17,18) was adopted to estimate the mean and standard error of free energy changes using the parseFEP plugin of the VMD package (2).

According to the thermodynamic cycle shown in Fig. S3, $\Delta\Delta G(Na^+ \rightarrow K^+)$ can be derived using the following equation,

$$\begin{aligned}\Delta\Delta G(Na^+ \rightarrow K^+) &= \Delta G_{binding}(K^+) - \Delta G_{binding}(Na^+) \\ &= \Delta G_{site}(Na^+ \rightarrow K^+) - \Delta G_{bulk}(Na^+ \rightarrow K^+),\end{aligned} \quad (1)$$

where $\Delta G_{binding}(K^+)$ and $\Delta G_{binding}(Na^+)$ are the binding free energies of K^+ and Na^+ at the site respectively, while $\Delta G_{site}(Na^+ \rightarrow K^+)$ and $\Delta G_{bulk}(Na^+ \rightarrow K^+)$ are the free energy changes in the $Na^+ \rightarrow K^+$ alchemical transformations which occur at the binding site and in the bulk solution respectively. In practice, both $\Delta G_{site}(Na^+ \rightarrow K^+)$ and $\Delta G_{bulk}(Na^+ \rightarrow K^+)$ were derived from FEP calculations, and finally the $\Delta\Delta G(Na^+ \rightarrow K^+)$ was estimated from their difference.

The $\Delta G_{bulk}(Na^+ \rightarrow K^+)$ is a reference value which will be subtracted from the $\Delta G_{site}(Na^+ \rightarrow K^+)$ estimated at various binding sites. Therefore it was estimated in advance, by mutating a Na^+ ion in 70 mM NaCl to K^+. The target ion was initially placed at the center of a water box with identical size to the Na_vRh simulation system (in Table S1). After electrostatic neutralization by 70 mM NaCl, the system (system 1 in Table S6) was equilibrated for 0.5 ns. In the FEP calculation, the reaction coordinate was stratified into 108 or 109 windows, which were evenly divided in the middle range of the reaction path ($0.01 < \lambda < 0.09$). When approaching both ends of the reaction coordinates, the window size was diminished to accelerate convergence. In each window, 20000 simulation steps were performed, among which the first 2000-step pre-equilibration was excluded from the free energy calculation. After averaging over the three independently repeated calculations, $\Delta G_{bulk}(Na^+ \rightarrow K^+)$ was

estimated to be 20.90 ± 0.07 kcal/mol (as shown in Table S6). However, the calculation result may vary upon the size of simulation system. To evaluate this effect, the same calculation was performed in a smaller system with a size of 32 × 32 × 32 $Å^3$ (system 2 in Table S6). The consistent results generated from two systems (in Table S6) indicate that $\Delta G_{bulk}(Na^+ \rightarrow K^+)$ is independent on the system size in this work. Ultimately, the result estimated in the system 1 (20.90 ± 0.07 kcal/mol) was adopted as a uniform reference value which was subtracted from all of the following FEP calculations to estimate the $\Delta\Delta G(Na^+ \rightarrow K^+)$.

Table S2 shows the FEP simulations conducted to evaluate the $\Delta\Delta G(Na^+ \rightarrow K^+)$ within the binding sites of the WT-Na_vRh and the DEKA mutant. The initial structures were manually taken either from equilibration simulations (simulation 1, 2, 5 in Table S1) or from the ABF simulations, and were then equilibrated for additional 2~4 ns before the FEP calculations. In the FEP calculation, the target ions (Na^+ and K^+) were allowed to freely sample within 1.5 Å around the binding site along the z-axis, and a force constant of 100 kcal/mol/$Å^2$ was applied when the ion left the allowed region. Except for the target ion and the pre-placed ions, all extracellular ions were restricted 13 Å away from the entrance of the SF, which was defined by the center of the backbone carbonyl carbons of Ser181. In the simulations of the DEKA mutant, the same constraint as described in the ABF simulation was applied to maintain the "on-state" of Lys180 side-chain. The reaction coordinate was stratified into 186 or 192 windows (Table S2). In each window, at least 30000 simulation steps were performed, among which the first 4000-step pre-equilibration was excluded from free energy calculation. The total simulation time for each single FEP calculation exceeded 12 ns. The detailed information is shown in Table S7 to demonstrate the scheme of stratification and the equilibration steps in each window for FEP calculations 8-15 (in Table S2). The corresponding parameters for FEP calculations 1-7 were adjusted slightly for better convergence. Eventually, the reference value ($\Delta G_{bulk}(Na^+ \rightarrow K^+)$ = 20.90 ± 0.07 kcal/mol) was subtracted from the $\Delta G_{site}(Na^+ \rightarrow K^+)$ values derived from FEP simulations to calculate $\Delta\Delta G(Na^+ \rightarrow K^+)$. In calculation 15, the highly Na^+/K^+ selective conformation was taken from the FEP calculation 13 and both Na^+ ions at

site 1 and site 2 are manually removed. A force constant of 10 kcal/mol/Å^2 was applied to the α-carbons of the protein to maintain this highly selective conformation.

Table S4 shows the FEP calculations conducted to evaluate the $\Delta\Delta G(Na^+ \rightarrow K^+)$ at the locations within the constriction site (shown in Fig. 3) in the SF of the DEKA and the DEAA mutant. The initial structures were taken from the two-dimensional ABF simulation trajectories, which were equilibrated for 1 ns before the FEP calculations. The SF structures and uninterested ions were constrained in the same manner as in the ABF calculation. In specific, all α-carbons of the extracted structure were positionally restrained by a force constant of 10 kcal/mol/Å^2 so as to maintain the backbone conformation. The target cations (Na^+ or K^+) were restrained within 1.5 Å along the z-axis and within 0.2 Å along the x- and y-axis around the corresponding central coordinates shown in Fig. 3 and Table S4, by a force constant of 100 kcal/mol/Å^2. The reaction coordinate was stratified in the same scheme as FEP calculations 1-7 in Table S2, and the simulation time for each point exceeded 15 ns.

Table S5 shows the FEP calculations conducted to evaluate the $\Delta\Delta G(Na^+ \rightarrow K^+)$ around a carboxylate group (in acetate) and a carbonyl group (in N-methylacetylamide or NMA) (Fig. S15). The model compounds (acetate and NMA) were solvated in a water box of 32 × 32 × 32 Å^3, and were harmonically restrained (by a force constant 0.5 kcal/mol/Å^2) at the center of the simulation cell. Later a Na^+ ion was placed around the model compounds. In the system of acetate, the Na^+ was restrained within 3 Å to the center of the carboxylate oxygens. In the system of well-chelated acetate, the Na^+ was restrained within 2.6 Å to both carboxylate oxygens. In the system of NMA, the ion was restrained within 3 Å from the carbonyl oxygen, and one chloride ion was added to neutralize the system. In the following FEP simulation after 1ns pre-equilibration, the Na^+ was then mutated to K^+ to evaluate the ion selectivity, using the same stratification scheme as the system 2 in Table S6. After averaging over three independently repeated simulations (Table S5), $\Delta\Delta G(Na^+ \rightarrow K^+)$ was finally derived by subtracting the reference value ($\Delta G_{bulk}(Na^+ \rightarrow K^+)$ = 20.90 ± 0.07 kcal/mol). The total simulation time for each independently repeated calculation exceeded 5 ns.

The coordination analysis

To analyze the interacting patterns between Na^+/K^+ and the carboxylate group, an acetate was solvated in a water box of 32 × 32 × 32 $Å^3$ and was harmonically restrained (by a force constant 10 kcal/mol/$Å^2$) at the center of the simulation cell. The cations were then restricted within 5 Å from the center of the carboxylate oxygens in the following equilibrium simulation. Each system was simulated for 7 ns after 1000 steps of minimization, among which the last 3 ns frames were used for later calculation. Among the snapshot in which the cation is within 3.0 Å from at least one carboxylate oxygen, the distances between the cation and both carboxylate oxygens were computed, and their difference was recorded. Finally, the distribution of distance difference was drawn for Na^+ and K^+ (Fig. S16C).

To analyze the coordination status of a cation in a perfect chelated-state, the above system containing one acetate was engaged again. The acetate was restrained to the center of the box (by a force constant 0.5 kcal/mol/$Å^2$). The cations were then constrained at identical distances to both carboxylate oxygens. The ion-oxygen distance was set to 2.2, 2.4, and 2.6 Å respectively (by a force constant of 5000, 1000, and 500 kcal/mol/$Å^2$ respectively) in three independent equilibrium simulations. All systems were simulated for 5 ns after 1000 steps of minimization, and the frames from the last 3 ns were used for coordination analysis. The number of coordinated oxygens (within 3.5 Å to the ion) was counted for both Na^+ and K^+ and was then fitted with a Gaussian distribution (Fig. S17). For both Na^+ and K^+, commensurate systems without the acetate were generated as controls to evaluate the coordination numbers of Na^+ and K^+ in free water.

Supplementary Figures

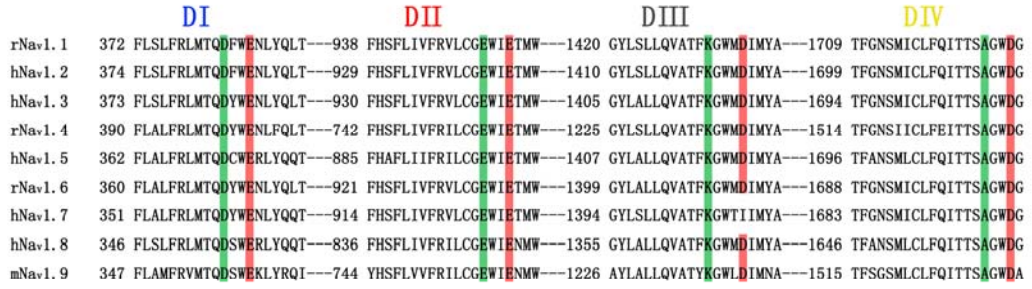

Figure S1. The sequence alignment for the SF regions from various mammalian Na_v channels. The source of the Na_v channels is labeled by the first letter in the name: "r" represents rat; "m" represents mouse; "h" represents human. The residues at the inner layer and the outer layer are shaded in green and red respectively.

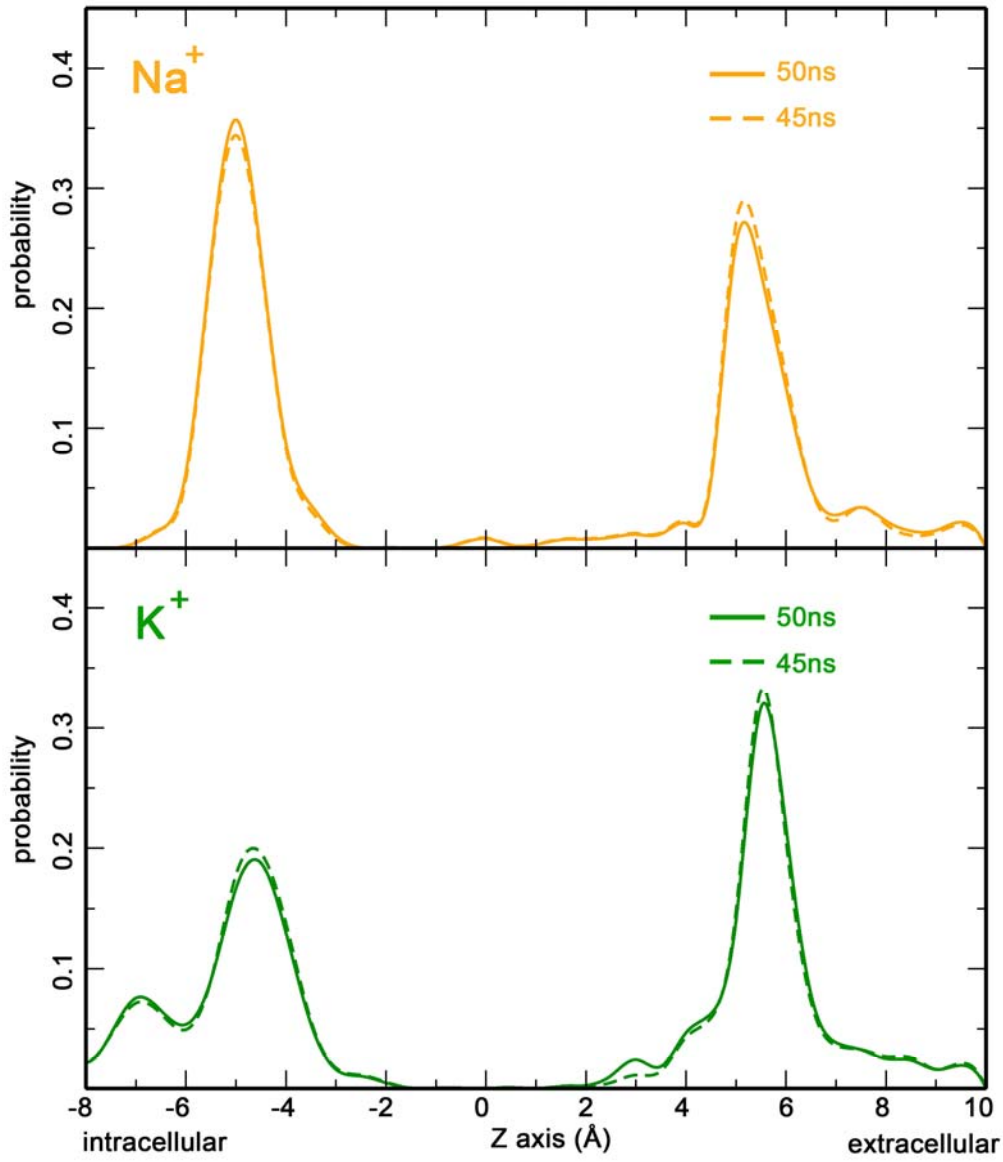

Figure S2. The residence probability profiles of Na^+ and K^+ along the permeation pathway in WT-Na_vRh calculated by frames from the overall 50 ns trajectories (solid) and the first 45 ns ones (dashed). The negligible difference between the curves indicates that the calculation has converged.

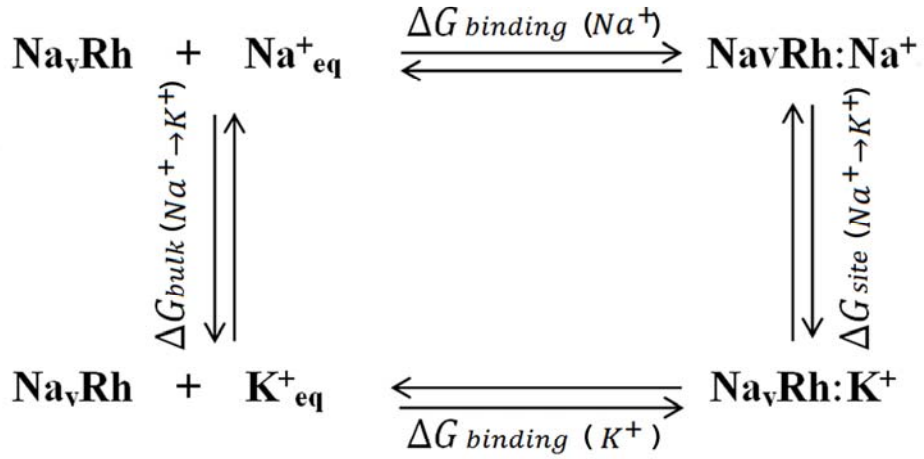

Figure S3. The protocol for FEP calculation.

According to the above thermodynamic cycle diagram, $\Delta\Delta G(Na^+ \rightarrow K^+)$ can be derived by subtracting $\Delta G_{bulk}(Na^+ \rightarrow K^+)$ from $\Delta G_{site}(Na^+ \rightarrow K^+)$. (see Eq. 1)

Positive $\Delta\Delta G(Na^+ \rightarrow K^+)$ values indicate Na^+ preference while negative $\Delta\Delta G(Na^+ \rightarrow K^+)$ values indicate K^+ preference at the site.

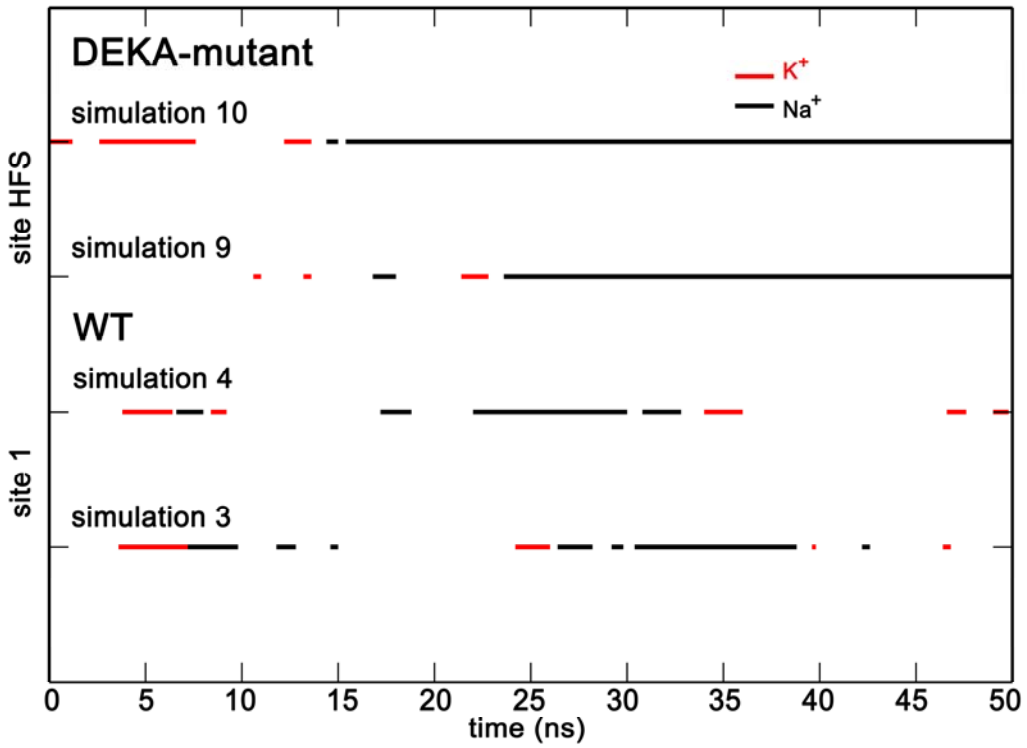

Figure S4. The ion competition at site 1 in the WT-Na_vRh (lower half) and site HFS in the DEKA mutant (upper half). Na^+ and K^+ ions bound in the according sites are labeled as black and red respectively. In the WT-Na_vRh, Na^+ and K^+ experienced frequent turnovers throughout the trajectory. In the DEKA mutant, a Na^+ won in both simulations after several rounds of turnovers, and resided in the site till the last frame of the trajectory.

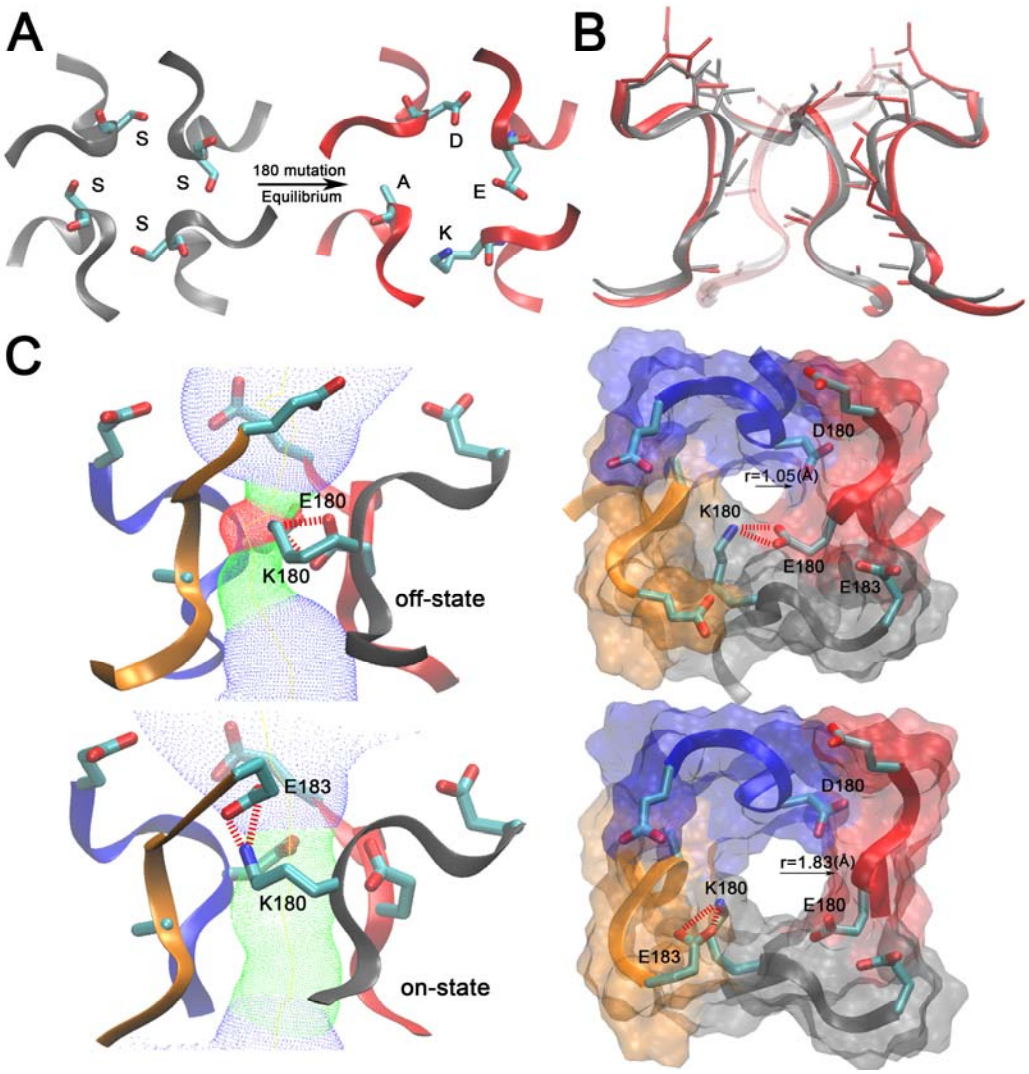

Figure S5. (A) The four Ser180 residues in Na_vRh are mutated to D, E, K and A respectively. (B) The structural superposition of backbone of the DEKA mutant (red) onto that of WT-Na_vRh (grey) suggests that the structure only changed slightly after mutation. (C) The side-chain of Lys180 has two states. At the "off-state" (upper panel), Lys180 side-chain protrudes into the pore to interact with the opposite Glu180 and blocks the ion penetration. At the "on-state" (lower panel), Lys180 side-chain points upward to interact with Glu183 in the neighboring chain (chain D). This conformation allows ion permeation. The pore size is shown by dots calculated using HOLE2 (http://www.csb.yale.edu/userguides/graphics/hole/doc/hole_d00.html). in the left panel (sideview) and by surface representation in the right panel (topview) respectively.

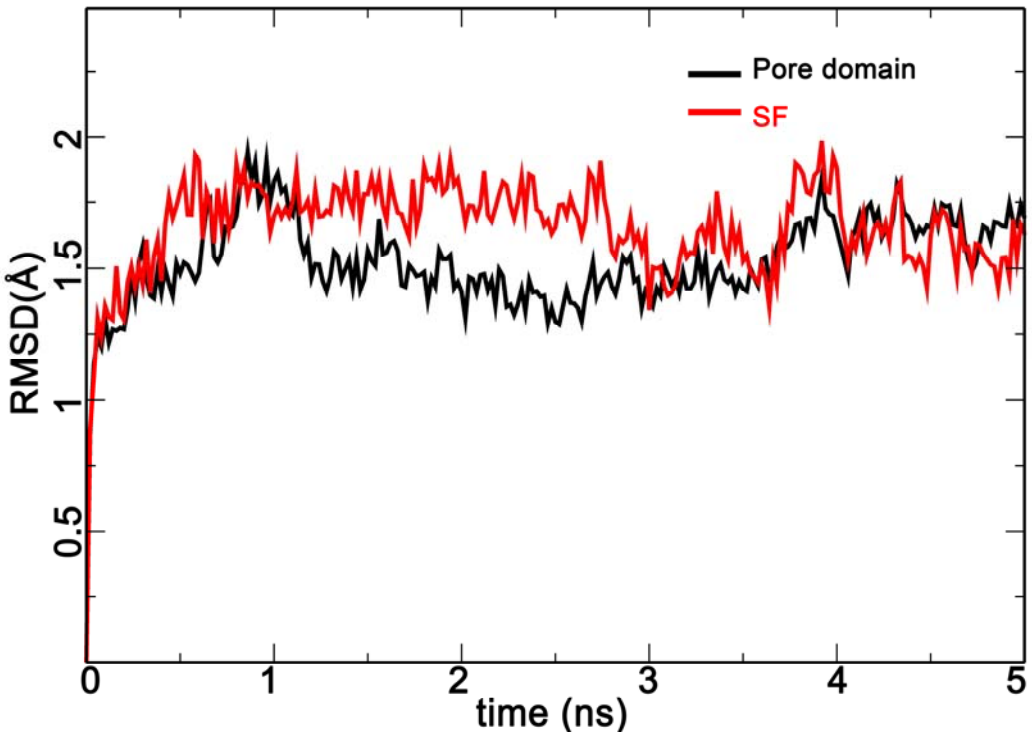

Figure S6. The root-mean-square-distance (RMSD) values for the backbone of SF (red) and the backbone of pore domain (black) never exceed 2 Å in the 5-ns equilibration after mutation.

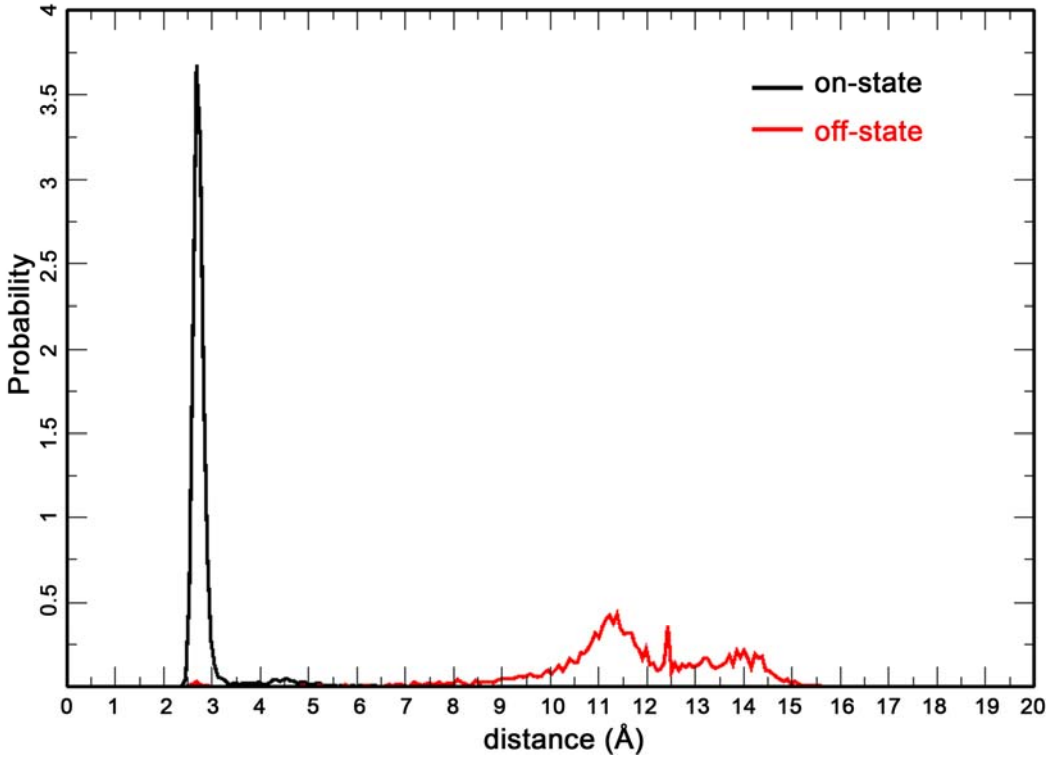

Figure S7. Distribution of the distance between the side-chain nitrogen of Lys180 (chain C) and the center of both carboxylate oxygens of Glu183 (chain D) measured from trajectories of successful (black) and failed (red) ion permeations.

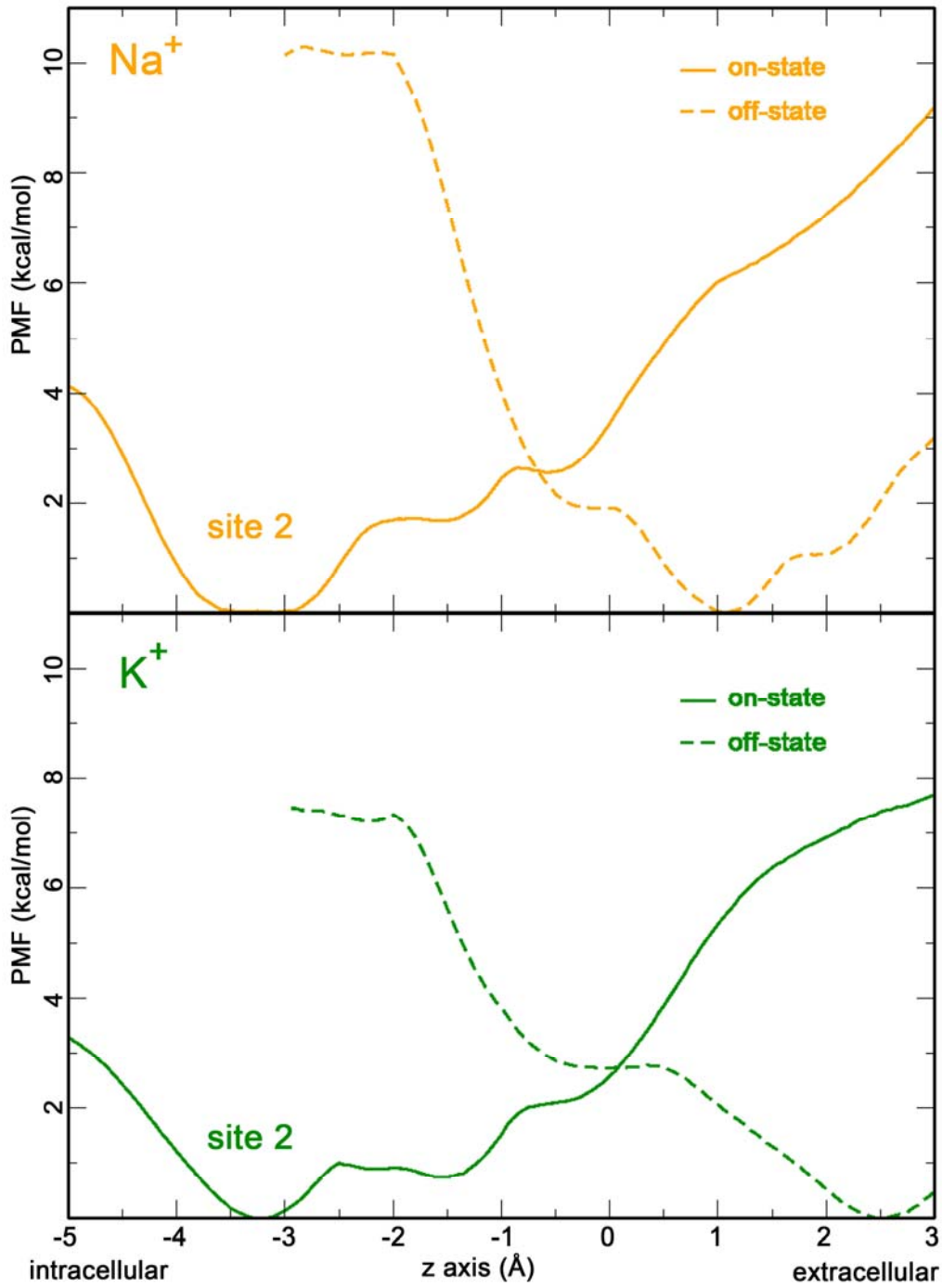

Figure S8. The free energy profiles are calculated for Na^+ (upper panel) and K^+ (lower panel) permeations using the ABF method when Lys180 side-chain is restrained to the "on-state" (solid) and the "off-state" (dashed) respectively.

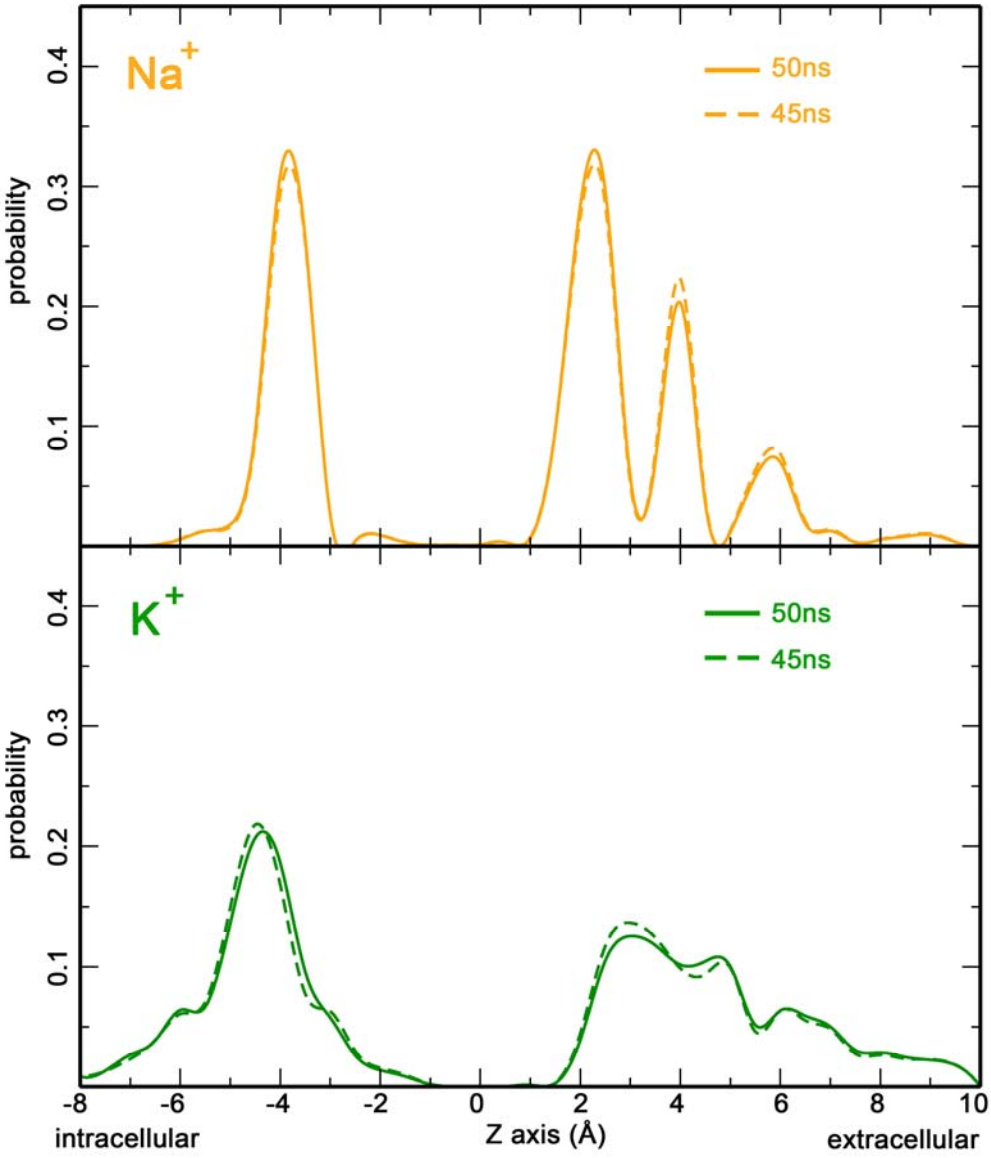

Figure S9. The residence probability profiles of Na^+ and K^+ along the permeation pathway in the DEKA mutant calculated by frames from the overall 50 ns trajectories (solid) and the first 45 ns ones (dashed). The negligible difference between the curves indicates that the calculation has converged.

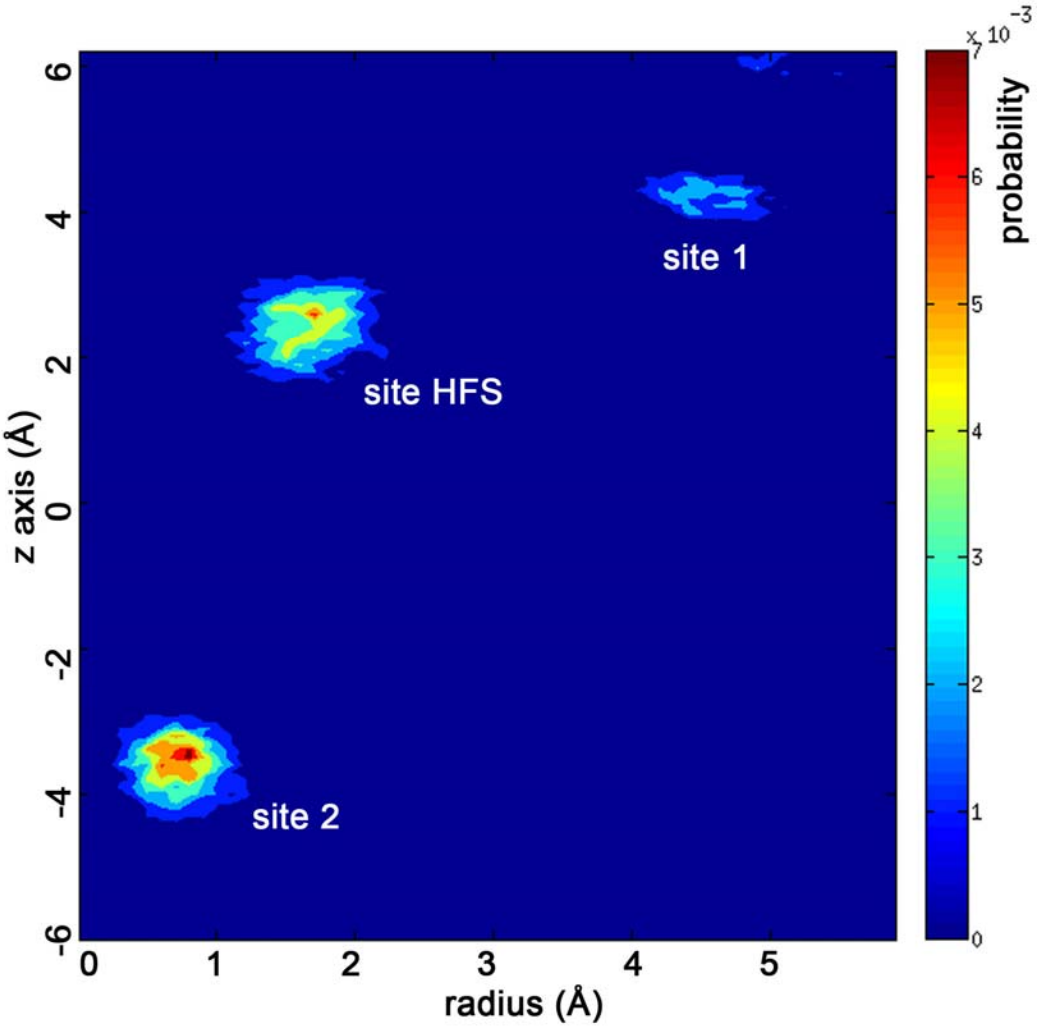

Figure S10. Two-dimensional probability distribution of Na^+ during its permeation through the SF of the DEKA mutant. The vertical axis is the permeation pathway (z-axis), while the horizontal axis represents the distance from the center of the pore in the plane perpendicular to the permeation pathway (xy-plane).

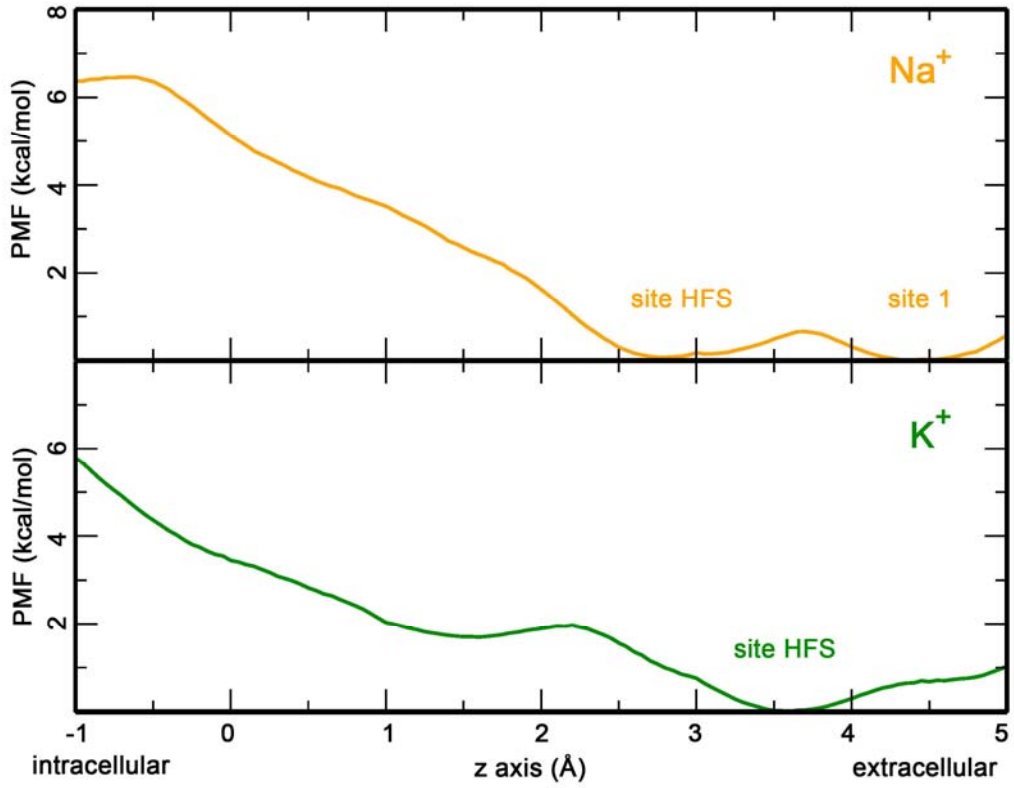

Figure S11. The free-energy profiles for the permeation of Na^+ (upper panel) and K^+ (lower panel) when the inner site (site 2) is pre-occupied by a cation.

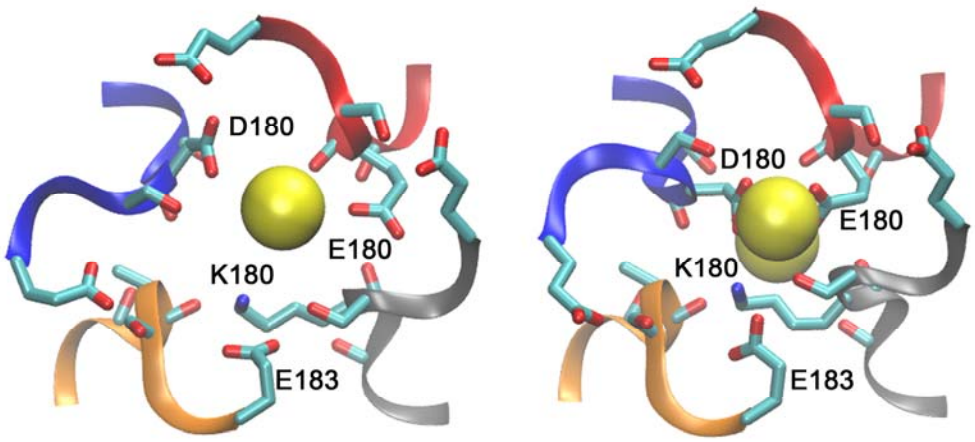

Figure S12. When the first ion passes through the constriction site, the carboxylate groups of Asp180 and Glu180 are spatially separated. (left panel) After the first ion occupies site 2, the arrival of the second ion at site HFS leads to a conformational change, by drawing the carboxylate groups of both Asp180 and Glu180 towards the ion. (right panel)

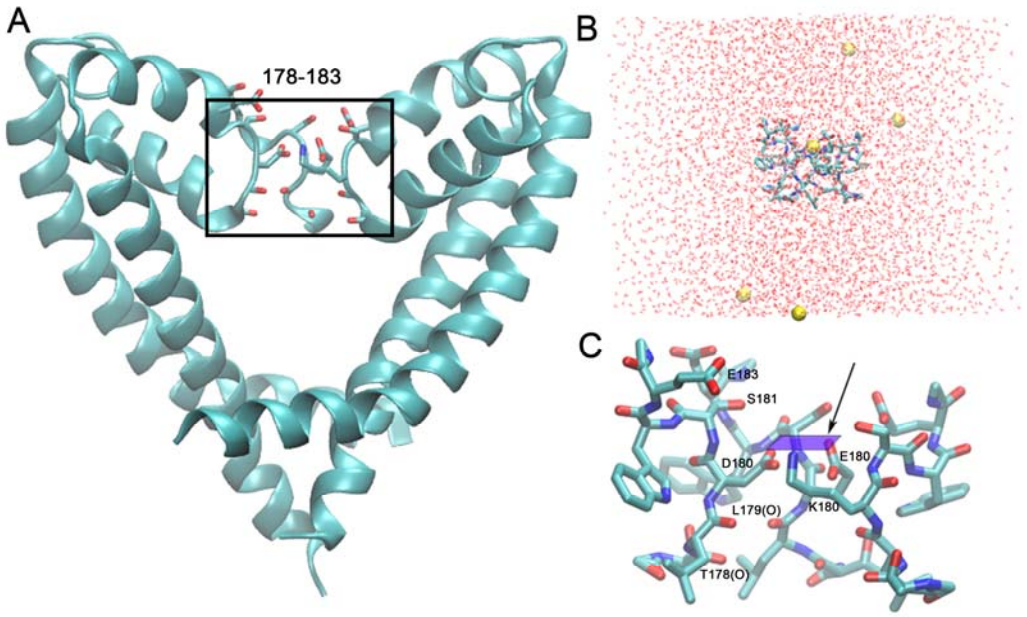

Figure S13. Procedure to calculate the two-dimensional free-energy profiles at the constriction site. The SF was extracted from the highly selective conformation (A) and was then immersed in explicit solvent (B). With strong positional restraints on the backbone of SF, a cation is allowed to sample in the plane of the constriction site (purple parallelogram indicated by the arrow in panel C).

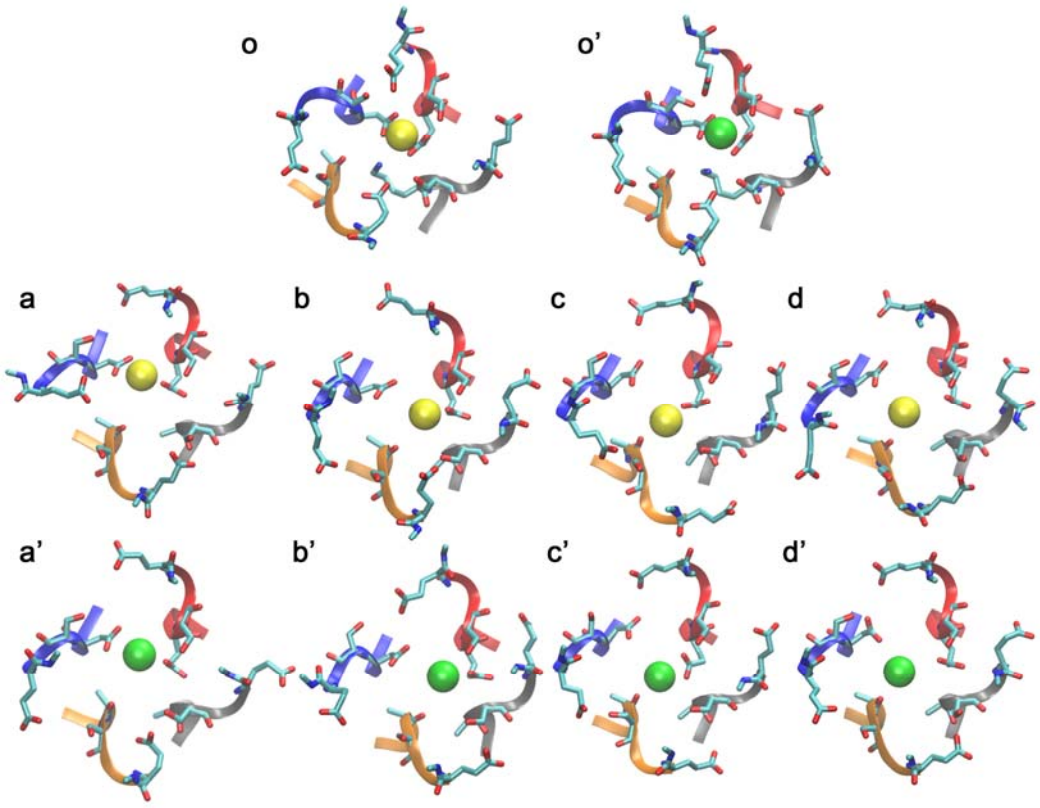

Figure S14. Representative structures taken from the 2D free-energy maps in Fig. 3. The structures are labeled identically to the local minima in Fig. 3C. Na^+ and K^+ are represented by yellow and green spheres respectively.

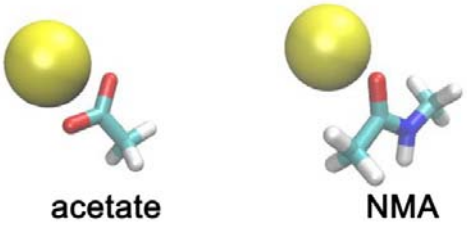

Figure S15. Acetate and NMA are adopted as the representative model compounds to explore the Na^+/K^+ selectivity of the carboxylate and carbonyl groups respectively.

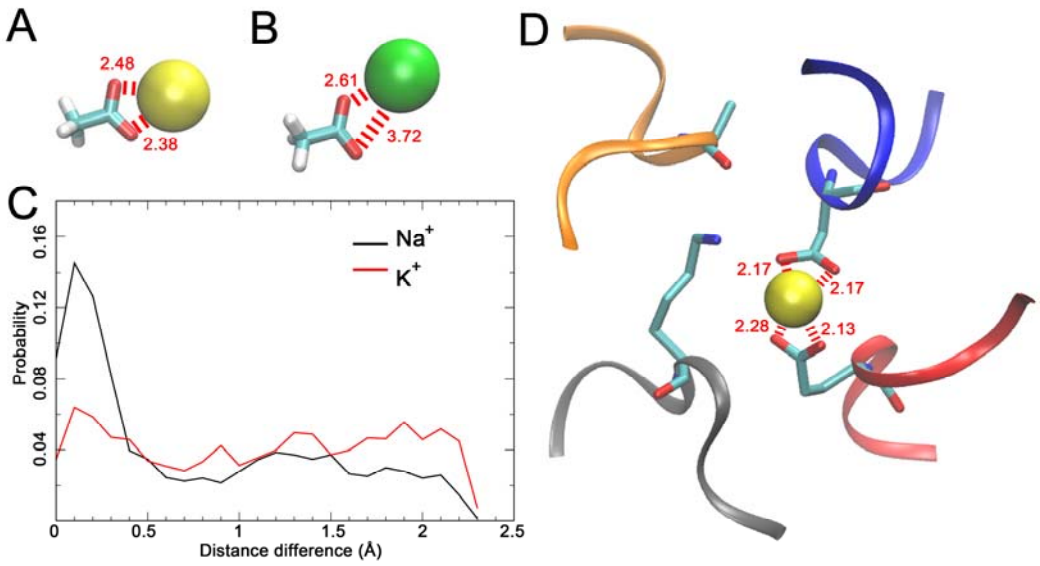

Figure S16. The interaction patterns between Na^+/K^+ and the carboxylate group. (A) Na^+ is well chelated by both carboxylate oxygens in the acetate. (B) K^+ frequently interacts closely only with one carboxylate oxygen. (C) The distribution of difference in the ion-oxygen distances shows that Na^+ (black) is more likely to bind the carboxylate group in a bi-dentate manner than K^+ (red). (D) The cation bound at site HFS in the DEKA mutant is usually well chelated by both carboxylate groups and most carboxylate oxygens are located within 2.4 Å to the cation.

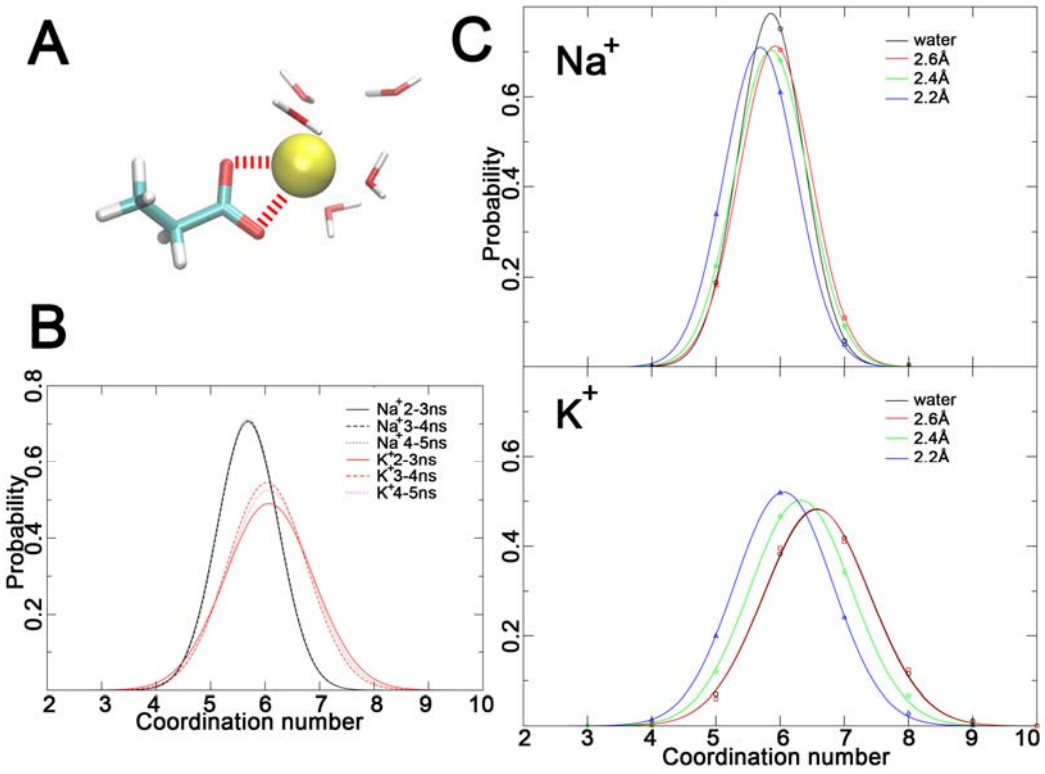

Figure S17. (A) Cations were constrained to locate at equal distances to both carboxylate oxygens to mimic the chelated state. Equilibrium simulations were then conducted at several constrained ion-oxygen distances (2.2, 2.4, and 2.6 Å), and the coordinated oxygens within 3.5 Å to the cation were counted and were fitted by Gaussian distribution. (B) The calculation on the coordination-distribution has converged, as indicated by the nearly identical curves obtained from 3 subsets of the simulation trajectories for both Na^+ and K^+. (C) The distribution of coordination numbers around Na^+ (upper panel) does not show marked shift upon the change of ion-oxygen distances. Na^+ keeps its ideal coordination state (as in water) at various distances. In contrast, the distribution of coordination numbers around K^+ (lower panel) shifts to left significantly upon the reduction of the ion-oxygen distance. K^+ loses its ideal coordination state (as in water) when ion-oxygen distance is less than 2.4 Å.

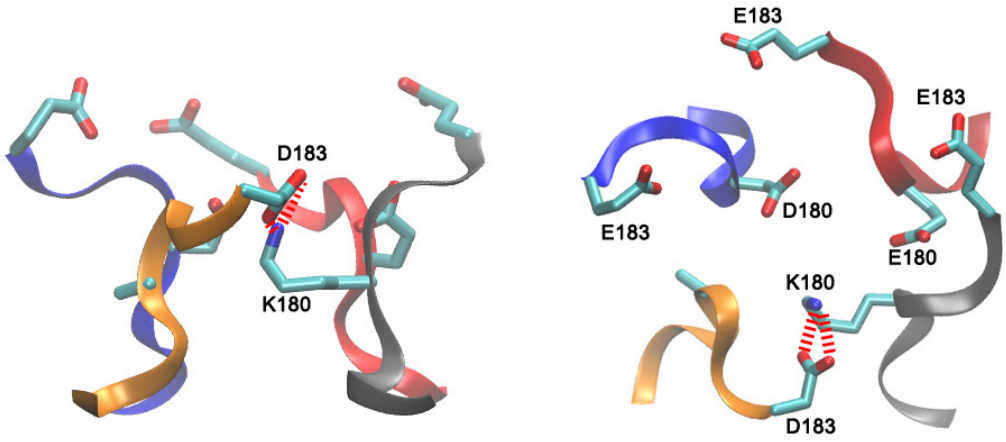

Figure S18. Asp183 (chain D) can interact with Lys180 (chain C) and hold the latter in the "on-state". The conformation is shown in sideview (left panel) and topview (right panel).

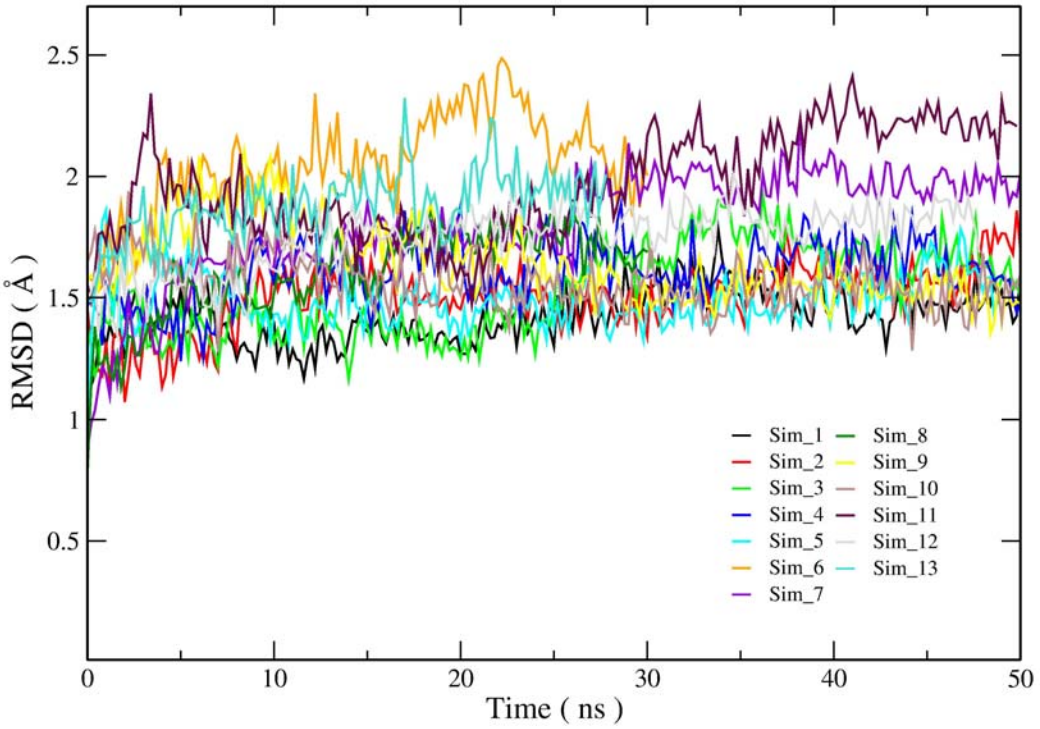

Figure S19. Trajectory RMSD for all equilibrium simulations enumerated in Table S1.

Supplementary Movies

Movie S1. WT-Na_vRh is permeable for Na^+ (yellow spheres).

Movie S2. WT-Na_vRh is permeable for K^+ (green spheres).

Movie S3. The DEKA mutant is impermeable when the Lys180 side-chain is at the "off-state". Both side-chains of Lys180 (chain C) and Glu183 (chain D) are represented as thick sticks. Na^+ ions are represented by yellow spheres.

Movie S4. When the Lys180 side-chain moves upward to the "on-state", the DEKA mutant becomes permeable. Both side-chains of Lys180 (chain C) and Glu183 (chain D) are represented as thick sticks. Na^+ ions are represented by yellow spheres.

Movie S5. Na^+ (yellow spheres) ions permeate through the DEKA mutant when the Lys180 side-chain is constrained at the "on-state".

Movie S6. K^+ (green spheres) ions permeate through the DEKA mutant when the Lys180 side-chain is constrained at the "on-state".

Movie S7. When the inner site (site 2) of the DEKA mutant is pre-occupied by a Na^+, equal concentrations of Na^+ (yellow spheres) and K^+ (green spheres) ions are allowed to compete for the site HFS.

Supplementary Tables

Table S1. Summary of equilibrium simulations

ID	Simulated protein	Ion centration	K180/R180 state	Open SF	Simulation time (ns)	First ion entering site 2	Probability of ion occupancy		
							Site 2	Site HFS	Site 1
1	WT	70 mM NaCl	NA	Yes	50	Na^+	Very high P	NA	Low P
2	WT	70 mM KCl	NA	Yes	50	K^+	Very high P	NA	Low P
3	WT	70 mM Na^+:K^+=1:1	NA	Yes	50	Na^+ (PIA)	Very high P	NA	Very low P
4	WT	70 mM Na^+:K^+=1:1	NA	Yes	50	K^+ (PIA)	Very high P	NA	Very low P
5	DEKA	70 mM NaCl	On	Yes	50	Na^+	Very high P	High P	Low P
6	DEKA	70 mM NaCl	Off	No	30	Ø	No	Low P	Very low P
7	DEKA	70 mM KCl	On	Yes	50	K^+	Very high P	Low P	Very low P
8	DEKA	70 mM KCl	Off	No	30	Ø	No	Low P	Very low P
9	DEKA	70 mM Na^+:K^+=1:1	On	Yes	50	Na^+ (PIA)	Very high P	High P(Na^+)	Very low P
10	DEKA	70 mM Na^+:K^+=1:1	On	Yes	50	K^+ (PIA)	Very high P	High P(Na^+)	Very low P
11	DEAA	70 mM NaCl	NA	Yes	50	Na^+	Very high P	High P	Very low P
12	DEAA	70 mM KCl	NA	Yes	50	K^+	Very high P	High P	Very low P
13	DEKA+ E183D(D)	70 mM NaCl	On	Yes	30	Na^+	Very high P	High P	Very low P

WT=wide type Na_vRh; DEKA=DEKA mutant; DEAA=DEAA mutant; DEKA+E183D(D)=DEKA mutant with Glu183 (chain D) mutated to Asp; NA=not available; PIA=placed in advance; Ø=unoccupied site; P=probability: very high > high > low > very low > no; (Na^+)=sodium ion can occupy the site stably.

Table S2. Detailed information for FEP calculations for WT-Na_vRh and the DEKA mutant

ID	$\Delta G_{site}(Na^+ \rightarrow K^+)$ for WT-Na_vRh (kcal/mol)			Forward (kcal/mol)	Backward (kcal/mol)	Simulation time (ns)	Number of windows	$\Delta\Delta G(Na^+ \rightarrow K^+)$ (kcal/mol)
	Site 1		Site 2					
1	21.60 ± 0.04		Ø	21.5658	21.6457	15.04	186	0.70 (0.08)
2	Ø		21.53 ± 0.04	21.2347	21.7981	15.64	186	0.63 (0.56)
3	21.64 ± 0.04		Na^+	22.0666	21.2178	14.24	186	0.74 (0.85)
4	20.94 ± 0.04		K^+	20.9874	20.8957	16.60	186	0.04 (0.09)
	$\Delta G_{site}(Na^+ \rightarrow K^+)$ for DEKA mutant (kcal/mol)							
	Site 1	Site HFS	Site 2					
5	21.64 ± 0.04	Ø	Ø	21.9132	21.3639	15.82	186	0.74 (0.55)
6	Ø	22.15 ± 0.04	Ø	22.9620	21.3141	14.72	186	1.25 (1.65)
7	Ø	Ø	21.58 ± 0.04	21.4942	21.6539	17.58	186	0.68 (0.16)
8	21.23 ± 0.04	Ø	Na^+	21.7343	20.8201	12.64	192	0.33 (0.91)
9	Ø	25.47 ± 0.04	Na^+	25.4721	25.5005	12.64	192	4.57 (0.03)
10	21.07 ± 0.04	Ø	K^+	21.2379	20.8444	12.64	192	0.17 (0.39)
11	Ø	23.28 ± 0.04	K^+	23.5703	23.1274	14.74	192	2.38 (0.44)
12	21.96 ± 0.05	Na^+	Na^+	22.5693	21.4515	12.64	192	1.06 (1.12)
13	Na^+	24.29 ± 0.04	Na^+	25.0050	23.5894	12.64	192	3.39 (1.42)
14	Na^+	Na^+	22.75 ± 0.04	23.3629	22.1505	12.64	192	1.85 (1.21)
15	(Na^+)	25.69 ± 0.05 (PR)	(Na^+)	26.4399	24.9259	12.64	192	4.79 (1.51)

Ø indicates unoccupied binding site; Na^+ and K^+ indicate the presence of these ions at the site; (Na^+) indicates that a Na^+ ion at the site was

removed; PR: the α-carbons of the SF were positional restrained to maintain the conformation; Forward: free energy estimated from the forward FEP calculation; Backward: free energy estimated from the backward FEP calculation; Simulation time: total time to complete the calculation; Number of windows: the number of windows used to stratify the reaction coordinate; $\Delta G_{site}(Na^+ \rightarrow K^+)$: free energy estimated by the Bennett acceptance ratio estimator; $\Delta\Delta G(Na^+ \rightarrow K^+)$: ion selectivity estimated by subtracting $\Delta G_{bulk}(Na^+ \rightarrow K^+)$ (20.90 ± 0.07 kcal/mol as shown in Table S6) from $\Delta G_{site}(Na^+ \rightarrow K^+)$. Numbers shown in the parenthesis listed in the last column are the uncertainties which are estimated by the difference between the forward and backward FEP calculations.

FEP calculations were labeled by the same ID values as Table 1. In specific, calculations 1-4 are performed for WT-Na_vRh while calculations 5-15 are performed for the DEKA mutant. Positive $\Delta\Delta G(Na^+ \rightarrow K^+)$ values indicate Na^+ preference while negative $\Delta\Delta G(Na^+ \rightarrow K^+)$ values indicate K^+ preference at the site.

Table S3. Analysis on ion occupancy time in competition simulations

Simulated protein	Tested site	Simulation ID	Ion pre-occupying Site 2	Tested ion	Number of bound ions	Ion occupancy time (ns)	p_value
WT	Site 1	3	Na^+	Na^+	11	1.5 ± 2.4	0.533
				K^+	8	1.0 ± 1.3	
		4	K^+	Na^+	10	1.4 ± 2.4	0.575
				K^+	10	1.0 ± 0.8	
DEKA	Site HFS	9	Na^+	Na^+	2	> 28.5	NA
				K^+	3	0.7 ± 0.6	
		10	K^+	Na^+	2	> 34.5	NA
				K^+	4	2.5 ± 2.1	

All simulations are labeled by the same ID as shown in Table S1; Number of bound ions: the number of corresponding ions present at the tested site along the trajectory; NA: not applicable for statistical test due to the lack of sufficient number of data points. ">": a single ion occupies the site and never leaves till the end of the trajectory, as shown in Fig. S4.

Table S4. FEP calculations for the SF of the DEKA and the DEAA mutants

Na_vRh mutants	Tested point	Constrained position	Forward (kcal/mol)	Backward (kcal/mol)	Simulation time (ns)	Number of windows	BAR estimator (kcal/mol)	$\Delta\Delta G(Na^+ \rightarrow K^+)$ (kcal/mol)
DEKA	o/o'	(0.7,1.2)	23.4720	22.4771	15.2	186	22.95 ± 0.04	2.05 (0.99)
DEAA	a/a'	(-1.3,1.3)	23.1466	22.6999	15.2	186	22.95 ± 0.04	2.05 (0.45)
	b/b'	(0.6,0.9)	22.1427	22.0075	15.2	186	22.06 ± 0.04	1.16 (0.14)
	c/c'	(0.6,-0.5)	22.5083	22.5404	15.2	186	22.54 ± 0.04	1.64 (0.03)
	d/d'	(-0.5,-0.5)	20.2033	19.4512	15.2	186	19.81 ± 0.04	-1.09 (0.75)

Constrained position: the initial position of the sampling cation in the plane (The positions of o/o', a/a', b/b', c/c', and d/d' are labeled in Fig. 3); Forward: free energy estimated from the forward FEP calculation; Backward: free energy estimated from the backward FEP calculation; Simulation time: total time to complete the calculation; Number of windows: the number of windows used to stratify the reaction coordinate; BAR estimator: free energy estimated by the Bennett acceptance ratio estimator; $\Delta\Delta G(Na^+ \rightarrow K^+)$: ion selectivity estimated by subtracting $\Delta G_{bulk}(Na^+ \rightarrow K^+)$ (20.90 ± 0.07 kcal/mol as shown in Table S6) from $\Delta G_{site}(Na^+ \rightarrow K^+)$. Numbers shown in the parenthesis listed in the last column are the uncertainties which are estimated by the difference between the forward and backward FEP calculations.

Stratification here is the same as FEP calculations 1-7 in Table S2.

Table S5. Ion-oxygen interactions in non-polarizable and polarizable force fields

$\Delta G_{site}(Na^+ \rightarrow K^+)$ (kcal/mol)		NMA	Acetate	Well-chelated acetate
#1	Forward	20.6406	21.7466	23.4505
	Backward	20.8194	21.6661	23.6593
	BAR estimator	20.76 ± 0.06	21.71 ± 0.06	23.59 ± 0.05
#2	Forward	20.4844	21.6825	23.5669
	Backward	20.7663	21.4773	23.5841
	BAR estimator	20.61 ± 0.05	21.60 ± 0.06	23.57 ± 0.06
#3	Forward	20.8243	21.5841	23.3980
	Backward	20.4346	21.5382	23.4159
	BAR estimator	20.62 ± 0.06	21.56 ± 0.06	23.41 ± 0.06
Average		20.66 ± 0.08	21.62 ± 0.08	23.52 ± 0.10
$\Delta\Delta G(Na^+ \rightarrow K^+)$		-0.24 ± 0.11	0.72 ± 0.11	2.62 ± 0.12

The calculations are repeated for three times, as indicated by #1, #2, and #3; Well-chelated acetate: ions restrained within 2.6 Å to both carboxylate oxygens; Forward: free energy estimated from the forward FEP calculation; Backward: free energy estimated from the backward FEP calculation; BAR estimator: free energy estimated by the Bennett acceptance ratio estimator; $\Delta\Delta G(Na^+ \rightarrow K^+)$: ion selectivity estimated by subtracting $\Delta G_{bulk}(Na^+ \rightarrow K^+)$ (20.90 ± 0.07 kcal/mol as shown in Table S6) from $\Delta G_{site}(Na^+ \rightarrow K^+)$.

The same stratification strategy as system 2 in Table S6 was adopted here, and the total simulation time for each independently repeated calculation was 5.392ns.

Table S6. Estimating the reference value $\Delta G_{bulk}(Na^+ \rightarrow K^+)$ in FEP calculations

$\Delta G_{bulk}(Na^+ \rightarrow K^+)$		Forward (kcal/mol)	Backward (kcal/mol)	Simulation time (ns)	Number of windows	BAR estimator (kcal/mol)	Average (kcal/mol)
System 1	#1	20.8728	20.6960	4.32	108	20.82 ± 0.06	**20.90 ± 0.07**
	#2	21.0195	20.7486	4.36	109	20.92 ± 0.05	
	#3	20.9159	20.9773	4.56	109	20.96 ± 0.06	
System 2	#1	20.9413	20.8675	4.32	108	20.92 ± 0.06	20.89 ± 0.04
	#2	20.8212	21.0008	8.64	108	20.91 ± 0.04	
	#3	20.8447	20.8690	8.64	108	20.85 ± 0.04	

Forward: free energy estimated from the forward FEP calculation; Backward: free energy estimated from the backward FEP calculation; Simulation time: total time to complete the calculation; Number of windows: the number of windows used to stratify the reaction coordinate; BAR estimator: free energy estimated by the Bennett acceptance ratio estimator; Average: free energy derived from averaging over the three independent calculations.

In system 1, $\Delta G_{bulk}(Na^+ \rightarrow K^+)$ was estimated in a water box with identical size to the simulated system (simulation 1 in Table S1). The calculation was repeated in a small water box of 32×32×32 $Å^3$ (system 2) to show that the calculated free energy change is independent on the size of the water box. In both systems, the calculation was performed for three times. In practice, the average $\Delta G_{bulk}(Na^+ \rightarrow K^+)$ value obtained from system 1 (shown as bold) was adopted in the later calculation to estimate $\Delta\Delta G(Na^+ \rightarrow K^+)$.

Table S7. Example of the stratification in FEP calculations

λ	[0,0.0001]	[0.0001,0.0005]	[0.0005,0.001]	[0.001,0.005]	[0.005,0.01]	[0.01,0.015]
Steps($\times 10^4$)	5	5	5	5	5	5
λ	[0.015,0.02]	[0.02,0.025]	[0.025,0.03]	[0.03,0.035]	[0.035,0.04]	[0.04,0.045]
Steps($\times 10^4$)	5	3	3	3	3	3
λ	[0.045,0.05]	[0.05,0.055]	[0.055,0.06]	[0.06,0.065]	[0.065,0.07]	[0.07,0.075]
Steps($\times 10^4$)	3	3	3	3	3	3
λ	[0.075,0.08]	[0.08,0.085]	[0.085,0.09]	[0.09,0.095]	[0.095,0.1]	[0.1,0.105]
Steps($\times 10^4$)	3	3	3	3	3	3
λ	[0.105,0.11]	[0.11,0.12]	[0.12,0.13]	[0.13,0.14]	[0.14,0.15]	[0.15,0.16]
Steps($\times 10^4$)	3	3	3	3	3	3
λ	[0.16,0.17]	[0.17,0.18]	[0.18,0.19]	[0.19,0.2]	[0.2,0.21]	[0.21,0.22]
Steps($\times 10^4$)	3	3	3	3	3	3
λ	[0.22,0.23]	[0.23,0.24]	[0.24,0.25]	[0.25,0.26]	[0.26,0.27]	[0.27,0.28]
Steps($\times 10^4$)	3	3	3	3	3	3
λ	[0.28,0.29]	[0.29,0.3]	[0.3,0.31]	[0.31,0.32]	[0.32,0.33]	[0.33,0.34]
Steps($\times 10^4$)	3	3	3	3	3	3
λ	[0.34,0.35]	[0.35,0.36]	[0.36,0.37]	[0.37,0.38]	[0.38,0.39]	[0.39,0.4]
Steps($\times 10^4$)	3	3	3	3	3	3
λ	[0.4,0.41]	[0.41,0.42]	[0.42,0.425]	[0.425,0.43]	[0.43,0.435]	[0.435,0.44]
Steps($\times 10^4$)	3	3	3	3	3	3
λ	[0.44,0.445]	[0.445,0.45]	[0.45,0.455]	[0.455,0.46]	[0.46,0.465]	[0.465,0.47]
Steps($\times 10^4$)	3	3	3	3	3	3
λ	[0.47,0.475]	[0.475,0.48]	[0.48,0.485]	[0.485,0.49]	[0.49,0.495]	[0.495,0.5]
Steps($\times 10^4$)	3	3	3	3	3	3
λ	[0.5,0.505]	[0.505,0.51]	[0.51,0.515]	[0.515,0.52]	[0.52,0.525]	[0.525,0.53]
Steps($\times 10^4$)	3	3	3	3	3	3
λ	[0.53,0.535]	[0.535,0.54]	[0.54,0.545]	[0.545,0.55]	[0.55,0.555]	[0.555,0.56]
Steps($\times 10^4$)	3	3	3	3	3	3
λ	[0.56,0.565]	[0.565,0.57]	[0.57,0.575]	[0.575,0.58]	[0.58,0.585]	[0.585,0.59]
Steps($\times 10^4$)	3	3	3	3	3	3
λ	[0.59,0.595]	[0.595,0.6]	[0.6,0.605]	[0.605,0.61]	[0.61,0.615]	[0.615,0.62]
Steps($\times 10^4$)	3	3	3	3	3	3
λ	[0.62,0.625]	[0.625,0.63]	[0.63,0.635]	[0.635,0.64]	[0.64,0.645]	[0.645,0.65]
Steps($\times 10^4$)	3	3	3	3	3	3
λ	[0.65,0.655]	[0.655,0.66]	[0.66,0.665]	[0.665,0.67]	[0.67,0.675]	[0.675,0.68]
Steps($\times 10^4$)	3	3	3	3	3	3
λ	[0.68,0.685]	[0.685,0.69]	[0.69,0.695]	[0.695,0.7]	[0.7,0.705]	[0.705,0.71]
Steps($\times 10^4$)	3	3	3	3	3	3
λ	[0.71,0.715]	[0.715,0.72]	[0.72,0.725]	[0.725,0.73]	[0.73,0.735]	[0.735,0.74]
Steps($\times 10^4$)	3	3	3	3	3	3
λ	[0.74,0.745]	[0.745,0.75]	[0.75,0.755]	[0.755,0.76]	[0.76,0.765]	[0.765,0.77]

Steps($\times 10^4$)	3	3	3	3	3	3
λ	[0.77,0.775]	[0.775,0.78]	[0.78,0.785]	[0.785,0.79]	[0.79,0.795]	[0.795,0.8]
Steps($\times 10^4$)	3	3	3	3	3	3
λ	[0.8,0.802]	[0.802,0.804]	[0.804,0.806]	[0.806,0.808]	[0.808,0.81]	[0.81,0.812]
Steps($\times 10^4$)	4	4	4	4	4	4
λ	[0.812,0.814]	[0.814,0.816]	[0.816,0.818]	[0.818,0.82]	[0.82,0.822]	[0.822,0.824]
Steps($\times 10^4$)	4	4	4	4	4	4
λ	[0.824,0.826]	[0.826,0.828]	[0.828,0.83]	[0.83,0.832]	[0.832,0.834]	[0.834,0.836]
Steps($\times 10^4$)	4	4	4	4	4	4
λ	[0.836,0.838]	[0.838,0.84]	[0.84,0.842]	[0.842,0.844]	[0.844,0.846]	[0.846,0.848]
Steps($\times 10^4$)	4	4	4	4	4	4
λ	[0.848,0.85]	[0.85,0.852]	[0.852,0.854]	[0.854,0.856]	[0.856,0.858]	[0.858,0.86]
Steps($\times 10^4$)	4	4	4	4	4	4
λ	[0.86,0.865]	[0.865,0.87]	[0.87,0.875]	[0.875,0.88]	[0.88,0.885]	[0.885,0.89]
Steps($\times 10^4$)	3	3	3	3	3	3
λ	[0.89,0.895]	[0.895,0.9]	[0.9,0.905]	[0.905,0.91]	[0.91,0.915]	[0.915,0.92]
Steps($\times 10^4$)	3	3	3	3	3	3
λ	[0.92,0.925]	[0.925,0.93]	[0.93,0.935]	[0.935,0.94]	[0.94,0.945]	[0.945,0.95]
Steps($\times 10^4$)	3	3	3	3	3	3
λ	[0.95,0.955]	[0.955,0.96]	[0.96,0.965]	[0.965,0.97]	[0.97,0.975]	[0.975,0.98]
Steps($\times 10^4$)	3	3	3	3	3	3
λ	[0.98,0.985]	[0.985,0.99]	[0.99,0.995]	[0.995,0.999]	[0.999,0.9999]	[0.9999,1]
Steps($\times 10^4$)	5	5	5	5	5	5

FEP calculations 8-10, 12-15 all followed the above schedule. In FEP calculations 1-7 and 11, the reaction coordinate was stratified in a slightly different manner. In specific, for the windows between 0.8 and 0.86, the window width was changed to 0.0025 rather than 0.002, and the simulation steps in some windows were extended for better convergence. Steps shown here in each window include 4000 steps of pre-equilibration, which were excluded from the final calculation.

Table S8. Independently repeated FEP calculations for the data in Table 1 and Table S2

ID	$\Delta\Delta G(Na^+ \rightarrow K^+)$ (kcal/mol)	
	#1	#2
1	0.70 (0.08)	0.26 (0.89)
2	0.63 (0.56)	1.24 (0.27)
3	0.74 (0.85)	0.71 (0.70)
4	0.04 (0.09)	-0.36 (0.52)
5	0.74 (0.55)	0.52 (0.15)
6	1.25 (1.65)	1.29 (1.89)
7	0.68 (0.16)	1.25 (0.15)
8	0.33 (0.91)	0.70 (0.07)
9	4.57 (0.03)	4.68 (1.64)
10	0.17 (0.39)	0.03 (1.54)
11	2.38 (0.44)	2.47 (1.83)
12	1.06 (1.12)	1.29 (0.35)
13	3.39 (1.42)	3.51 (1.49)
14	1.85 (1.21)	1.76 (0.95)
15	4.79 (1.51)	4.98 (1.55)

Column #1 is identical to the results listed in Table 1 and Table S2, while column #2 shows the values derived from independently repeated calculations. The uncertainties which are roughly estimated from the difference between the forward and backward FEP calculations are listed in the parenthesis.

Table S9. FEP re-calculation using different force field parameters

	Forward (kcal/mol)	Backward (kcal/mol)	Simulation time (ns)	Number of windows	BAR estimator (kcal/mol)	$\Delta\Delta G(Na^+ \rightarrow K^+)$ (kcal/mol)
Water system 1	17.8809	17.9529	4.32	108	17.93 ± 0.05	---
Water system 2	18.0735	18.0472	4.32	108	18.03 ± 0.05	---
ID 9 in Table1	22.8731	22.4812	13.74	192	22.67 ± 0.04	4.74 (0.39)
DEKA o/o'	20.2394	20.1398	15.2	186	20.20 ± 0.04	2.27 (0.10)
DEAA d/d'	17.0033	16.3926	15.2	186	16.69 ± 0.03	-1.24 (0.61)

In the table, the ion parameter set was taken from the research of Joung et al. (19) such that the difference of solvation energy between Na^+ and K^+ can better reproduce the experimental value (-17 kcal/mol) (20,21). Numbers shown in the parenthesis listed in the last column are the uncertainties which are estimated by the difference between the forward and backward FEP calculations.

Reference

1. Zhang, X., M. Xia, Y. Li, H. Liu, X. Jiang, W. Ren, J. Wu, P. Decaen, F. Yu, S. Huang, J. He, D.E. Clapham, N. Yan & H. Gong. Analysis of the selectivity filter of the voltage-gated sodium channel Na(v)Rh. *Cell Res* **23**, 409-422 (2013).
2. Humphrey, W., A. Dalke & K. Schulten. VMD: Visual molecular dynamics. *Journal of Molecular Graphics* **14**, 33-38 (1996).
3. Phillips, J.C., R. Braun, W. Wang, J. Gumbart, E. Tajkhorshid, E. Villa, C. Chipot, R.D. Skeel, L. Kalé & K. Schulten. Scalable molecular dynamics with NAMD. *J Comput Chem* **26**, 1781-1802 (2005).
4. MacKerell, A.D., D. Bashford, Bellott, R.L. Dunbrack, J.D. Evanseck, M.J. Field, S. Fischer, J. Gao, H. Guo, S. Ha, D. Joseph-McCarthy, L. Kuchnir, K. Kuczera, F.T.K. Lau, C. Mattos, S. Michnick, T. Ngo, D.T. Nguyen, B. Prodhom, W.E. Reiher, B. Roux, M. Schlenkrich, J.C. Smith, R. Stote, J. Straub, M. Watanabe, J. Wiórkiewicz-Kuczera, D. Yin & M. Karplus. All-Atom Empirical Potential for Molecular Modeling and Dynamics Studies of Proteins†. *The Journal of Physical Chemistry B* **102**, 3586-3616 (1998).
5. Corry, B. Na+/Ca2+selectivity in the bacterial voltage-gated sodium channel NavAb. *PeerJ* **1**, e16 (2013).
6. Martyna, G.J., D.J. Tobias & M.L. Klein. Constant pressure molecular dynamics algorithms. *The Journal of Chemical Physics* **101**, 4177-4189 (1994).
7. Feller, S.E., Y. Zhang, R.W. Pastor & B.R. Brooks. Constant pressure molecular dynamics simulation: The Langevin piston method. *The Journal of Chemical Physics* **103**, 4613-4621 (1995).
8. Essmann, U., L. Perera, M. Berkowitz, T. Darden, H. Lee & L. Pedersen. A smooth particle mesh Ewald method. *The Journal of Chemical Physics* **103**, 8577-8593 (1995).
9. Miyamoto, S. & P. Kollman. Settle: An analytical version of the SHAKE and RATTLE algorithm for rigid water models. *Journal of Computational Chemistry* **13**, 952-962 (1992).
10. Darve, E. & A. Pohorille. Calculating free energies using average force. *The Journal of Chemical Physics* **115**, 9169-9183 (2001).
11. Darve, E., M. Wilson & A. Pohorille. Calculating Free Energies Using a Scaled-Force Molecular Dynamics Algorithm. *Molecular Simulation* **28**, 113-144 (2002).
12. Rodriguez-Gomez, D., E. Darve & A. Pohorille. Assessing the efficiency of free energy calculation methods. *The Journal of Chemical Physics* **120**, 3563-3578 (2004).
13. Darve, E., D. Rodriguez-Gomez & A. Pohorille. Adaptive biasing force method for scalar and vector free energy calculations. *The Journal of Chemical Physics* **128**, 144120 (2008).
14. Zwanzig, R.W. High-Temperature Equation of State by a Perturbation Method. II. Polar Gases. *The Journal of Chemical Physics* **23**, 1915-1922 (1955).
15. Kollman, P. Free energy calculations: Applications to chemical and biochemical phenomena. *Chemical Reviews* **93**, 2395-2417 (1993).
16. Zacharias, M., T.P. Straatsma & J.A. McCammon. Separation‐shifted scaling, a new scaling method for Lennard‐Jones interactions in thermodynamic integration. *J. Chem. Phys.* **100**, 9025-9031 (1994).
17. Bennett, C.H. Efficient estimation of free energy differences from Monte Carlo data. *Journal of Computational Physics* **22**, 245-268 (1976).
18. Pohorille, A., C. Jarzynski & C. Chipot. Good Practices in Free-Energy Calculations. *The Journal*

of Physical Chemistry B **114**, 10235-10253 (2010).

19. Joung, I.S. & T.E. Cheatham. Determination of Alkali and Halide Monovalent Ion Parameters for Use in Explicitly Solvated Biomolecular Simulations. *The Journal of Physical Chemistry B* **112**, 9020-9041 (2008).
20. Marcus, Y. Thermodynamics of solvation of ions. Part 5.-Gibbs free energy of hydration at 298.15 K. *Journal of the Chemical Society, Faraday Transactions* **87**, 2995-2999 (1991).
21. Schmid, R., A.M. Miah & V.N. Sapunov. A new table of the thermodynamic quantities of ionic hydration: values and some applications (enthalpy-entropy compensation and Born radii). *Physical Chemistry Chemical Physics* **2**, 97-102 (2000).